Transport Properties of SINIS Junctions With High-Current Density

F. Born, D. Cassel, K. Ilin, A. M. Klushin, M. Siegel, A. Brinkman, A. A. Golubov, M. Yu. Kupriyanov, and H. Rogalla

***Abstract*—We have fabricated $Nb/Al_2O_3/Al/Al_2O_3/Nb$ devices with different current densities using a conventional fabrication process, varying pressure and oxidation time. Patterning of the multilayers was done using standard photolithography and electron-beam lithography. The current density of SINIS junctions was changed in the range from 0.5 kA/cm^2 to 20 kA/cm^2. We achieved characteristic voltages up to 0.35 mV. By fabricating sub-μm junction with a width from 0.1 μm to 0.5 μm, we have studied the influence of the asymmetry of barriers on transport properties. By comparing the experimental and theoretical temperature dependence of the characteristic voltage we estimated the barrier transparency and its asymmetry. The comparison shows a good agreement of experimental data with the theoretical model of tunnelling through double-barrier structures in the dirty limit. A new approach for determination of the asymmetry of both barriers based on the measurement of the electrostatic field distribution in the SINIS structure has been developed.**

***Index Terms*—Josephson junctions, double-barrier structures, integrated circuits.**

I. Introduction

APPLICATIONS of Josephson junctions in integrated circuits for Rapid-Single-Flux Quantum (RSFQ) logic and voltage metrology require devices with nonhysteretic current-voltage characteristics (IVC). Standard $Nb/Al_2O_3/Nb$ tunnel junctions should be shunted with an external shunt to achieve a value of the McCumber parameter $\beta_C < 1$. External shunts reduce the characteristic voltage of Josephson junctions and have dimensions from several μm up to 50 μm. The additional required wiring leads to parasitic inductances. One concept to achieve nonhysteretic IVC is to increase the Josephson current density, J_c, above 10^2 kA/cm^2 [1], [2].

A typical example of structures of this class are the well known $Nb/Al/AlO_x/Nb$ tunnel devices [3]. An increase in the critical current density in these structures is considered now as one of the mainstream development in superconductive sub-μm junction technology [4]. Experimental and theoretical studies of high-J_c Josephson tunnel junctions [5], [6] have demonstrated the excellent agreement between the experimental data and the results of the Multiple-Andreev Reflection (MAR) theory combined with the Schepp-Bauer distribution of transparencies [7]. It is important that the distribution [5], [6] was derived for the first time for a system that is physically very much different from one disordered interface. These results demonstrate that artificially prepared Al-oxide interfaces in high-J_c Josephson tunnel junctions with critical current density of the order of 200 kA/cm^2 can be characterized by the effective suppression parameter γ_B.

This approach is also valuable for describing ballistic double-barrier SINIS structure with symmetric uniform tunnel barriers. These are intrinsically shunted structures with an intermediate layer consisting of a thin Al layer, see references in [8]. At Physikalisch-Technische Bundesanstalt, SINIS junctions have been successfully implemented in Josephson voltage standard circuits. A high level of complexity has been reached by integrating up to 70 000 Josephson junctions [9]. A 10 V constant voltage step has been reached showing that the parameter spread of the SINIS junctions was rather small.

Two important parameters of SINIS junctions are the critical temperature of the N interlayer and the suppression parameter of the Cooper pair density at the interfaces [10] which is mainly controlled by the transparency of the interfaces. We have performed a systematic study of the influence of the barrier transparency on critical current, I_C, and normal resistance, R_N, by preparing SIS and SINIS junctions under identical technological conditions and comparing their transport properties.

It is important to note that the advantages of SIS'IS structures can be used to improve the reproducibility of SIS devices. It is sufficient to prepare SIS'IS structures with barriers having an one order of magnitude different interface transparency. In this case a simple method for estimation of the level of asymmetry of the transparency is needed. We have developed a new approach to determine the asymmetry by measuring the decay length of the electrical field in the SINIS structure and comparing it with the solution of the Laplace equation.

II. Transport Model

A. Josephson Current

In the frame of the microscopic theory of superconductivity it was shown [10]–[12] that for a small interlayer thickness d (compared to its decay length $\xi_{\rm nd}$) the super-current $I(\varphi)$ across an SINIS structure has the following form

$$\frac{I(\varphi)R_N}{2\pi T_C} = \frac{T}{T_C\gamma_{\rm eff}}\left\{\sum_{\omega>0}\frac{f^2}{\omega^2+f^2}\frac{\pi T_C}{\Omega}\right\}\sin(\varphi) + \frac{T}{T_C}\left\{\sum_{\omega>0}\frac{f}{\sqrt{\omega^2+f^2}}\frac{\Delta}{\Omega}\right\}\frac{\sin(\varphi)}{\eta(\varphi)}, \quad (1)$$

Manuscript received August 6, 2002. The work was supported in part by the Russian State Contract FTN-20(00)-P, ISTC 1199, INTAS 97-1712, DFG Si 704/1-2, and Office of Navel Research Grant N00014-00-1-0025.

F. Born, D. Cassel, K. Ilin, A. M. Klushin, and M. Siegel are with Institut für Schichten und Grenzflaechen, Forschungzentrum Juelich GmbH, Juelich 52425 Juelich, Germany (e-mail: m.siegel@fz-juelich.de).

A. Brinkman, A. A. Golubov, and H. Rogalla are with Department of Applied Physics, University of Twente, 7500 AE Enschede, The Netherlands.

M. Yu. Kuprianov is with Institute of Nuclear Physics, Moscow State University, 119899 GSP Moscow, Russian Federation.

Digital Object Identifier 10.1109/TASC.2003.814160

where

$$\Omega = \sqrt{\omega^2(1+q)^2 + (fq\eta(\varphi) + \Delta)^2},$$
$$\eta(\varphi) = \sqrt{\cos^2(\varphi) + \gamma_-^2 \sin^2(\varphi)},$$
$$q = \frac{\pi T_C g}{\omega \gamma_{\text{eff}}}, \quad \gamma_- = \frac{\gamma_{B1} - \gamma_{B2}}{\gamma_{B1} + \gamma_{B2}} \tag{2}$$

Here, f and g are the absolute values of Green's functions in the superconductive banks, $\omega = \pi T(2n+1)$ are the Matsubara frequencies and Δ is the modulus of the order parameter of the interlayer which should satisfy the self-consistency equation

$$\Delta \left\{ \ln \frac{T}{T_C^*} + 2\pi T \sum_{\omega>0} \left[\frac{1}{\omega} - \frac{1}{\Omega} \right] \right\} = 2\pi T \sum_{\omega>0} \left[\frac{fq\eta(\varphi)}{\Omega} \right] \tag{3}$$

Here, T_C^* is the critical temperature of the interlayer material.

The parameter γ_{eff} describes the overall resistance of the structure and characterizes its $I_C R_N$ product. It is defined by:

$$\gamma_{\text{eff}} = \frac{\gamma_{B1} \cdot \gamma_{B2}}{\gamma_{B1} + \gamma_{B2}} \cdot \frac{d}{\xi_{\text{nd}}},$$
$$\xi_{\text{nd}} = \sqrt{\frac{D}{2\pi T_C}}, \quad \gamma_{B1,2} = \frac{R_{B1,2}}{\rho_N \cdot \xi_{\text{nd}}} \tag{4}$$

Here, $D = v_F l/3$ and ρ_N are the diffusion coefficient (v_F is Fermi velocity, l is electron mean free path) and resistivity of the S'-interlayer, correspondingly, T_C is the critical temperature of the S electrodes, $R_{B1,2}$ are the specific boundary resistances at the interfaces between S and S' electrodes.

The asymmetry of both barriers was included in the SINIS model in [8]. The characteristic voltage of junctions is strongly influenced by the asymmetry parameter γ_- which is defined in (2) as shown in Fig. 1. The characteristic voltage can be enhanced or reduced by increasing the transparency of one barrier. This effect depends on temperature and γ_{eff}, see Fig. 1. In the case of large γ_{eff} an increase of asymmetry leads to a reduction of characteristic voltage, see upper part of Fig. 1. The opposite effect is appears for small γ_{eff} (lower part of Fig. 1.).

B. Electrostatic Field Distribution

Because of different conductivities of the metallic thin films s (Al, Nb) of the multilayer structure an injected current will be redistributed on a certain characteristic length within these structures. The characteristic length of this redistribution depends on the interface resistance of the lower oxide barrier. The distribution of electrostatic field caused by an injected dc-current in a multilayer structure can be calculated by solving the Laplace equation with appropriate boundary conditions. In detail, this solution will be published elsewhere [13]. The schematic view of devices suitable for field distribution measurements is shown in Fig. 2. The top electrode is separated into several sub-μm lines of the width w. The two inner lines are used for current injection and the others for measurement of voltage drops. The z-axis indicates the symmetry of our structure ($x = 0$). The distribution will be measured on one side, e.g., $x < 0$, at a temperature of $T = 10$ K in a normal four-point measurement. The exterior electrode will be used as the ground electrode. We have supposed that the injected current is distributed uniformly across the surface of both inner electrodes. Under the assumption that the thickness of all films is smaller than their planar dimensions we can neglect the planar field distribution. The field distribution along the negative part of the x-axis is given by the following solution

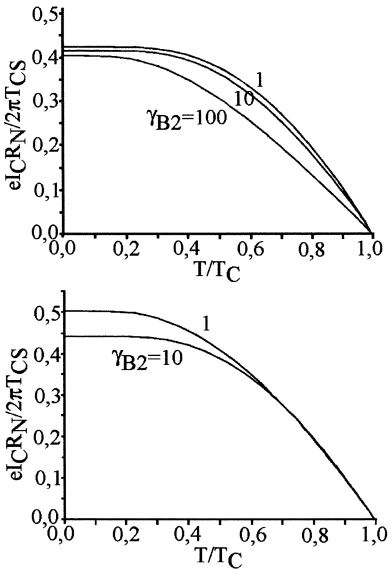

Fig. 1. Theoretical dependence of normalized $I_C R_N$ product on temperature of a SINIS junction with asymmetric barriers for fixed γ_{B1} and different γ_{B2}.

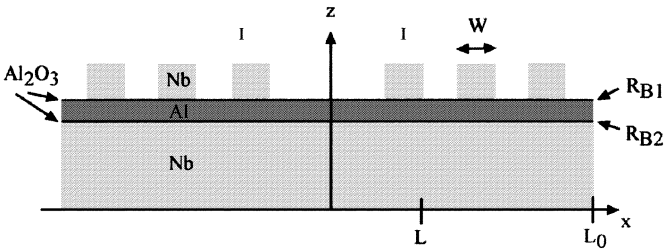

Fig. 2. Schematic view of a SINIS structure with separated-sub-μm-top electrodes for measurement of the electrostatic field distribution.

$$V_N \propto \exp\{\kappa x\}, \kappa = \pm\sqrt{\frac{1}{R_{B2}} \frac{\sigma_N d_N + \sigma_S d_S}{\sigma_N d_N \sigma_S d_S}} \tag{5}$$

The decay length κ describes the characteristic length where the injected current is redistributed. The redistribution depends on interface resistance R_{B2} and conductivities σ_S, σ_N of the superconductive and normal layers in the multilayer structure. The conductivities and thickness of all layers may be determined independently. Therefore, measurements of the decay length κ allow us to determine the interface resistance R_{B2}. The asymmetry of both barriers can be determined comparing the interface resistances determined from measurements of γ_{eff} and κ.

III. Fabrication

We have fabricated $Nb/Al_2O_3/Al/Al_2O_3/Nb$ devices using the conventional Selective Niobium Anodization Process

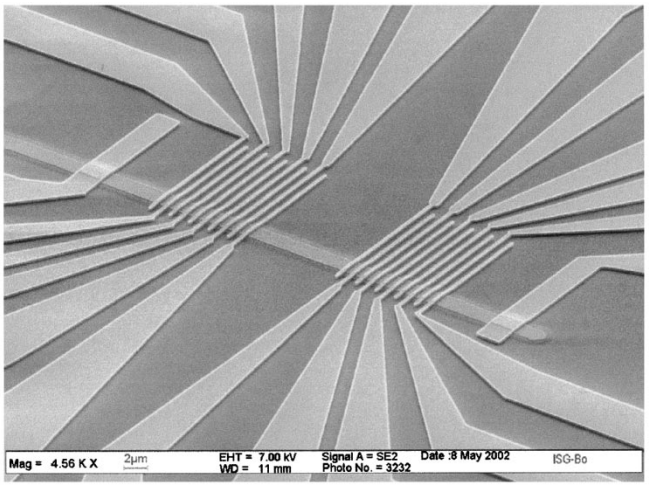

Fig. 3. SEM picture of a SINIS device fabricated with electron-beam lithography. The width of the middle multilayer finger is 2 μm and the width of the top electrodes is 0.3 μm.

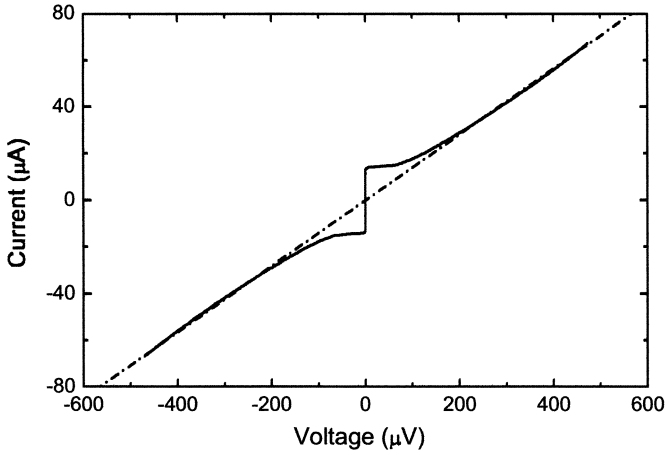

Fig. 4. Current-voltage characteristic of a SINIS junction at $T = 4.2$ K, an area of 4 μm^2, $J_C = 380$ A/cm^2, $R_N = 7\ \Omega$ and $I_C R_N = 100\ \mu$V.

(SNAP) [14]. The multilayer Nb/Al_2O_3/Al/Al_2O_3/Nb were deposited on an cooled oxidized 2-inch Si wafer by dc sputtering with a base pressure less than 10^{-6} mbar. The thickness of the Nb base and top electrodes were 100 nm and 30 nm, respectively. The thickness of the Al middle electrode was 10 nm and was kept constant. The tunnel barriers were formed by thermal oxidation in pure oxygen at room temperatures. Oxidation is the crucial step in the fabrication process of double-barrier structures. The exposure parameter $p \times t$ (where p is the oxygen pressure in the chamber and t the oxidation time of the Al layers) commonly used for barrier fabrication must have extremely small values [15]–[18]. To achieve different current densities the pressure and oxidation time have been changed from 10^{-3} to 10^{-1} mbar and 1 min to 30 min, respectively. The oxidation was performed in the deposition chamber. The main disadvantage of this approach is that the residual oxygen pressure in the chamber may play a significant role for the success of the whole fabrication process. In particular, it may influence the critical temperature T_C^* of the Al interlayer, increasing its value to about 2.7 K [19]. The increase of T_C^* is a consequence of changes in the transport properties of thin interlayer Al. The larger is T_C^*, the closer the film to the dirty limit. Differences in the crystalline structure and surface morphology between the first Al layer deposited on the base Nb electrode and the second interlayer Al layer deposited on the lower Al_2O_3 barrier may cause changes in the growth of the first and second Al_2O_3 barriers even if they are grown under the same thermodynamic conditions. Thus, we may have a difference in the transparency of both tunneling barriers, which is difficult to control. To minimize these influences we have used a Nb pre-sputtering step to reduce partial pressure of oxygen before deposition of the next layer. In the SINIS fabrication process the oxidation was performed in a continuous oxygen gas flow. This makes short oxidation times, exact pressure control, and low desorption rates of residual gases possible.

The patterning of all devices with structures up to a few micrometers has been performed by conventional contact photolithography. To prepare the base electrode the Nb/Al_2O_3/Al/Al_2O_3/Nb multilayer was patterned by lift-off. Then the wafers were anodized. The anodization was stopped at voltages of 47 V. Afterwards the 300 nm thick top electrode and wiring layer were deposited by dc sputtering and patterned by lift-off. Devices with sub-μm top electrodes were patterned using electron-beam lithography and reactive-ion etching. Fig. 3 shows a SEM picture of a device with a 0.3 μm wide top electrodes for measurements of the electrical field distribution.

The electrical measurements were performed by standard four-point measurements with a PC based data acquisition system measured using GoldExl software [20]. The measurements of temperature dependencies of the critical current in the range of 0.3 K to 8 K have been made in He^3 cryostat.

IV. Experimental Results

A. Current-Voltage Characteristics

Fig. 4 shows the current-voltage characteristic of a SINIS junction with $J_C = 380$ A/cm^2. At $T = 4.2$ K all junctions with $J_C < 1$ KA/cm^2 exhibit a nearly hysteretic-free IVC. At small voltages, $eV \leq \Delta_{\rm Nb}/\gamma_{\rm eff} \ll \Delta_{\rm Nb}$ the IVC looks rather similar to the IVC predicted by the RSJ model. At larger voltages the dc current across the structures becomes a nonlinear function of applied voltage with a strong increase of current at $eV \propto \Delta_{\rm Nb}$. We have fabricated some special high-resistance devices to be measured above the gap voltage. An example of an IVC is shown in Fig. 5. The parameters are $I_C = 0.5\ \mu$A and $R_N = 3.6\ \Omega$. The junction reveals a clear deficit current. This deficit current can be explained by MAR [21]. Additionally, we have shown the sub-gap resistance (marked with a dotted line). The asymptotic line in the small voltage range determines the normal resistance R_N of the device. We have measured the microwave power dependence of Shapiro steps and showed that the sub-gap resistance really determines the damping of the Josephson junction. The asymptotic line in the large voltage range represents the resistance of the junction caused by the two oxide barriers. We call it R_B.

The normal resistance decreases for increasing temperature and reaches finally the value of R_B in the limit $T \to T_C$.

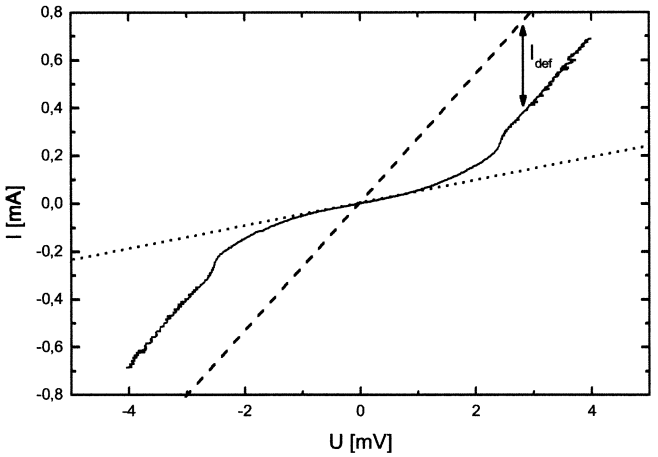

Fig. 5. Current-voltage characteristic of a 4 μm^2 SINIS junction with $I_C < 0.5$ μA at $T = 4.2$ K. The deficit current is marked in the viewgraph. The dotted line represents the sub-gap resistance of $R_N = 21.7$ Ω, the dashed line represents the voltage drop caused by the two barriers, $R_B = 3.8$ Ω.

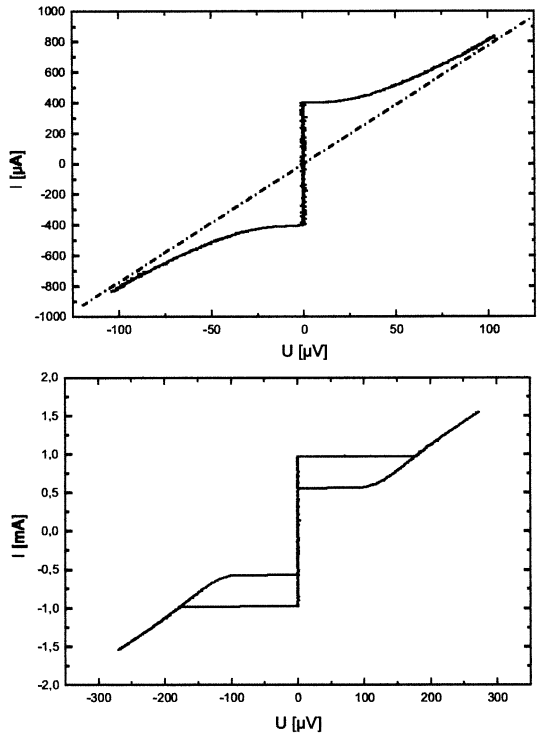

Fig. 6. Current-voltage characteristics of a 10 μm^2 SINIS junction, $T = 5.1$ K, $J_C = 11$ kA/cm^2.

The homogeneity of Josephson current distribution in the devices was evaluated by measurements of the magnetic field dependence of critical current, so-called Fraunhofer pattern. All junction in a wide range of current densities from 10 A/cm^2 to 20 KA/cm^2 reveal a clear Fraunhofer pattern showing a homogeneous Josephson current distribution.

It is important to note that the spread of critical currents of double-barrier junctions on a wafer was practically half an order of magnitude smaller compared to the spread of SIS devices. The on-chip spread of SINIS devices reaches about from 3% to 5%. The chip-to-chip spread was significantly higher. This can be explained by the fact, that deposition of the Al thin films and its oxidation was done in the same vaccum chamber. After oxidation of the first Al-film the deposition chamber was evacuated for 60 minutes (see previous paragraph). Some residual oxygen may influence the second oxidation process. The adjustment of the oxidation parameters p times t (pressure and time) was not as accurate as it should be by using of separate chambers.

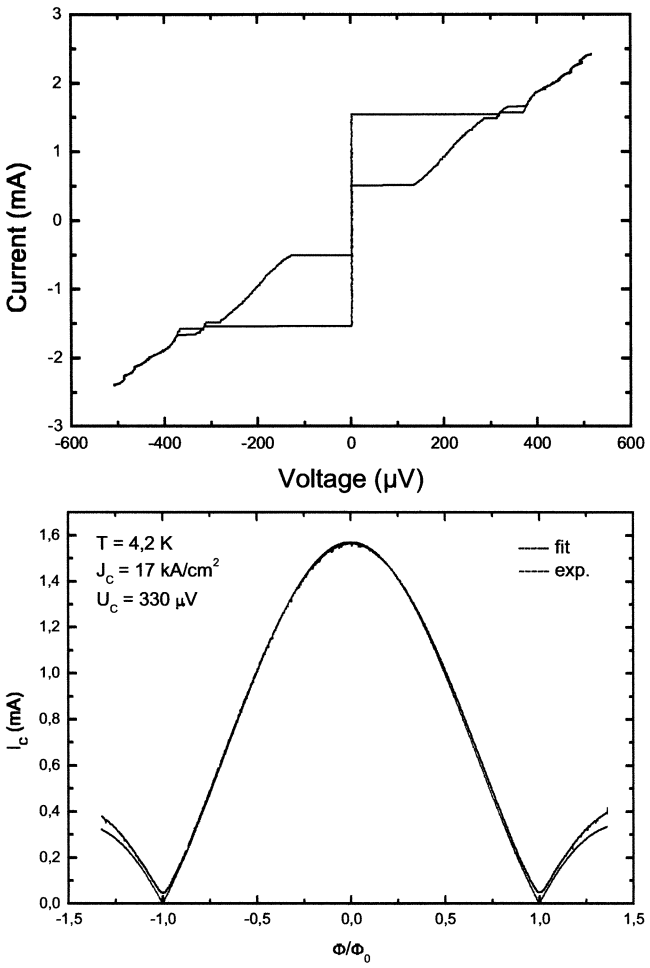

Fig. 7. Current-voltage characteristic (upper viewgraph) of a SINIS junction with $J_C = 17$ kA/cm^2 at $T = 4.2$ K and corresponding magnetic field dependence of critical current (lower viewgraph).

B. Temperature Dependence

The influence of temperature on IVC for a junction with high-current density is shown in Fig. 6. The junction has a current density of 17 kA/cm^2 at 4.2 K. The IVC in Fig. 6 shows a substantial hysteresis at 5.1 K. The area of this junction was 10 μm^2. Another example of a device with a high current density of $J_C = 16.5$ kA/cm^2 is shown in Fig. 7.

The characteristic voltage was 300 μV at 4.2 K. The homogeneous current distribution is shown by the ideal Fraunhofer pattern as shown in Fig. 7.

The suppression parameter γ_{eff} was determined from the temperature dependence of the $I_C R_N$ product and comparison with numerical simulation, see Fig. 8. Assuming symmetrical barriers γ_{eff} values of 300 and 80 have been determined. Depending on real oxidation conditions of both barriers we have found that the asymmetry parameter γ_- was varying from 0 for barriers

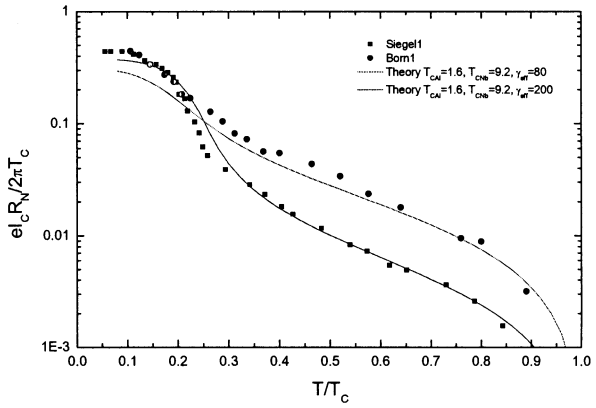

Fig. 8. Temperature dependence of normalized $I_C R_N$ product for two different SINIS junctions. Theoretical fit was performed for $\gamma_- = 0, \gamma_{\text{eff}} = 80$, and $\gamma_{\text{eff}} = 200$.

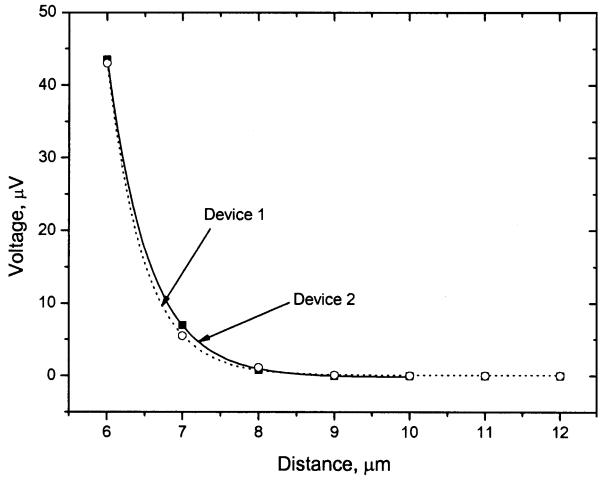

Fig. 9. Dependence of voltage on distance of two SINIS junctions with an identically prepared lower barrier. The point represent measured data. The lines represent an exponential fit according (5) with $\kappa = 2\ \mu\text{m}^{-1}$ (device 1) and $\kappa = 1.9\ \mu\text{m}^{-1}$ (device 1).

with low transparency to 0.2 for barriers with high transparency. We like to point out that for these devices the oxidation conditions for both barriers were identical. Thus the asymmetry is cause by differences in oxidation kinetics of the lower and upper Al film. We believe that mainly differences in the micro-crystalline structure and morphology of both Al layers are responsible for these differences.

C. Electrical Field Distribution

Based on the method described in the previous paragraph we have measured the distribution of the electrostatic field in SINIS devices. Using this method the interface resistance of the lower barrier can be determined. The conductivity of the Nb and Al layers was measured directly in special samples. At $T = 10$ K the conductivity of our Nb films was $\sigma_S = 0.14 - 10^6\ (\Omega\text{cm})^{-1}$. The conductivity of our Al interlayer was $\sigma_N = 1.5 - 10^6\ (\Omega\text{cm})^{-1}$.

The electrostatic field distribution was measured for several samples prepared according to Figs. 2 and 3. The voltage was measured between the sub-μm top electrodes in a four point set-up. Fig. 9 shows the voltage at different distances from the injection electrode I, see Fig. 2. A clear exponential decay of the voltage has been observed for all samples. The solid lines show the fitted curve according to (5). The decay length was $\kappa = 1.9\ \mu\text{m}^{-1}$ and $\kappa = 2.0\ \mu\text{m}^{-1}$ for the two junctions., respectively. The oxidation conditions of the lower barrier were identical and the upper barrier of device 2 was oxidized 10 times longer. Using (5) for R_B we have calculated an specific interface resistance of the lower barrier for $d_{\text{Nb}} = 70$ nm and $d_{\text{Al}} = 10$ nm of $R_{B2} = 0.5 \cdot 10^{-8}\ \Omega\text{cm}^2$.

Comparing the real resistances of two devices which have been calculated from the total resistance and the field distribution we obtain the following results for the resistance of the upper and lower barrier R_1 and R_2, respectively. One junction exhibits $R_1 \approx 1.58\ \Omega$ and $R_2 \approx 0.02\ \Omega$ and the second junction has $R_1 \approx 3\ \Omega$ and $R_2 \approx 0.03\ \Omega$. Thus, we conclude that the lower barrier has a significantly higher transparency than the upper barrier.

V. Conclusion

We have fabricated SINIS Josephson junctions with current densities from 10 kA/cm^2 to 26 kA/cm^2 and $I_C R_N$ products up to 350 μV at $T = 4,2$ K. The on-chip spread of critical currents of SINIS devices reaches about 3% for $J_C < 500$ A/cm^2 and 10% for devices with higher current densities.

The current-voltage characteristics of junction with $J_C < 500$ A/cm^2 behave close to the RSJ model. Devices with high current densities reveal still a hysteresis between 10% and 50%.

The transport properties in a wide temperature range can be described in terms of the SINIS theory in the dirty limit.

A new approach for determination of the asymmetry of both barriers based on the measurement of the electrostatic field distribution in the SINIS structure has been developed. We conclude that the transparency of the lower barrier in our junction technology is between 2 and 4 times larger in case of identical oxidation conditions.

For future enhancement of the characteristic voltage of SINIS devices the oxidation conditions of both barriers should be different to increase the influence of the proximity effect on the intermediate Al layer. Based on this approach, characteristic voltages up to 1 mV should be possible.

References

[1] V. Patel, S. K. Tolpygo, W. Chen, and J. E. Lukens, *Extended Abstracts ISEC-99*, Berkley, CA, USA, 1999, p. 229.
[2] V. Patel and J. E. Lukens, *IEEE Trans. Appl. Supercond.*, vol. 9, p. 3247, 1999.
[3] G. L. Kerber, L. A. Abelson, M. L. Leung, Q. P. Herr, and M. W. Johnson, *IEEE Trans. Applied Superconductivity*, vol. 11, pp. 1061–1065, 2001.
[4] Applications of Superconductivity (1999). [Online]. Available: http://pavel.physics.sunysb.edu/RSFQ/publications.html
[5] Y. Navech, D. Averin, and K. Likharev, Abstracts of ASC-2000, 4EL03, in IEEE Tran. Appl. Supercond., 2001. to be published.
[6] Y. Naveh, V. Patel, D. V. Averin, K. K. Likharev, and J. E. Lukens, Universal Distribution of Transparencies in Highly Conductive Nb/AlO_x/Nb Junctions. Preprint cond-mat/0 006 153.
[7] K. M. Schep and G. E. W. Bauer, *Phys. Rev. Lett.*, vol. 78, p. 3015, 1997. Phys. Rev. B 56, 15 860 (1997).
[8] D. Cassel, G. Pickartz, M. Siegel, E. Goldobin, H. H. Kohlstedt, A. Brinkmann, A. A. Golubov, M. Yu. Kuprianov, and H. Rogalla, *Physica C*, p. 350, 2001. 2001.
[9] H. Schulze, R. Behr, J. Kohlmann, F. Müller, and J. Niemeyer, Supercond. Sci. Technol., Mar. 2000. submitted to.

[10] M. Yu. Kupriyanov, A. Brinkman, A. A. Golubov, M. Siegel, and H. Rogalla, *Physica C*, vol. 16, pp. 326–327, 1999.
[11] M. Yu. Kupriyanov and V. F. Lukichev, *Sov. Phys. JETP*, vol. 67, p. 1163, 1988.
[12] A. V. Zaitsev, *Physica C*, vol. 2539, pp. 185–189, 1991.
[13] F. Born, "University Koeln," Diploma Thesis, July 2002.
[14] H. A. Huggins and M. Gurvitch, *J. Appl. Phys.*, vol. 57, p. 2103, 1985.
[15] L. Capogna and M. G. Blamire, *Phys Rev. B*, vol. 53, p. 5683, 1996.
[16] M. Maezawa and A. Shiji, *Appl. Phys. Lett.*, vol. 70, p. 3603, 1997.
[17] H. Sugiyama, A. Yanada, M. Ota, A. Fujimaki, and H. Hayakawa, *Jpn. J. Appl. Phys.*, vol. 36, p. L1157, 1997.
[18] D. Balashov, F.-I. Buchholz, H. Schulze, M. I. Khabipov, R. Dolata, M. Yu. Kupriyanov, and J. Niemeyer, *Supercond. Sci. Technol.*, vol. 13, p. 244, 2000.
[19] P. Nevirkovets, J. B. Ketterson, and S. Lomatch, *App. Phys. Lett.*, vol. 74, p. 1624, 1999.
[20] , E. Goldobin. [Online]. Available: http://www.geocities.com/goldexi
[21] Brinkman, *IEEE Trans. Appl. Supercond.*, vol. 1, p. 11, 2001.